Influence of Reactive Compatibilization on the Melt Flow Properties and Morphology of Polyamide 6/Styrene-Acrylonitrile Blends

*Christian Sailer, Ulrich Alexander Handge**

Summary: In this study, we investigate the influence of reactive compatibilization on the rheological properties of polyamide 6/styrene-acrylonitrile (PA 6/SAN) blends in the melt. Linear viscoelastic shear oscillations, simple elongation to a large stretch ratio and subsequent recovery experiments were performed. The morphology of the blends was examined by atomic force microscopy. We prepared three PA 6/SAN blends with different composition ratios of PA 6 and SAN (70/30, 50/50, 30/70) and a constant concentration of the reactive agent. Our experiments revealed that reactive compatibilization significantly increases the complex modulus of PA 6/SAN blends at low frequencies. In particular, the data of the PA 6/SAN 50/50 blend and the PA 6/SAN 30/70 blend indicated that an elastic network between neighbouring PA 6 domains was formed. In simple elongation, the transient elongational viscosity of the blends exceeded the values of the single components. In recovery, the recovered stretch of all blends was larger than the recovered stretch of the pure components. The differences of the blend morphology and of the linear viscoelastic behaviour were qualitatively explained by the asymmetric properties of the reactively compatibilized interface.

Keywords: blends; extensional rheology; reactive compatibilization; viscoelastic properties

Introduction

Polymer blending is an established technique to design new materials which combine advantageous properties of different polymers. However, since most polymer pairs are immiscible, compatibilization of the blends is necessary in order to obtain technologically relevant materials. Reactive compatibilization is based on the formation of the interfacial agent by a chemical reaction in-situ during melt mixing. It improves the end-use properties of blends of immiscible polymers by reducing the average size of the domains, decreasing coarsening of the morphology, and enhancing the interfacial adhesion between the blend components.[1] An important example for commercially available reactively compatibilized blends are blends of polyamide 6 (PA 6) and acrylonitrile-butadiene-styrene (ABS). For these blends the reactive coupling of PA 6 and maleic anhydride functionalized styrenic components leads to a fine morphology and improves the mechanical properties of the materials.[2–4] In contrast to the mechanical properties, only a few studies investigated the melt rheology of reactively compatibilized PA 6/ABS blends.[5]

Whereas the influence of the interfacial tension on the linear and non-linear rheology of uncompatibilized blends has been elucidated in detail,[6–9] in this study we focus on reactively compatibilized blends. In contrast to foregoing works which were mainly devoted to shear in the linear viscoelastic regime,[5,10,11] we investigate the melt flow properties of reactively

Institute of Polymers, Department of Materials, ETH Zurich, Wolfgang-Pauli-Strasse 10, 8093 Zurich, Switzerland
Fax: +41 44 632 10 76
E-mail: ulrich.handge@mat.ethz.ch

compatibilized blends in linear viscoelastic shear oscillations, in melt elongation to a large stretch ratio, and in subsequent recovery. By analyzing the elastic and viscous properties of the blends, we examine the properties of the reactively compatibilized interface. In our previous study similar PA 6/SAN blends with varying SANMA concentration were investigated.[12] In this work the absolute concentration of the reactive agent is constant for all blends.

Experimental Part

Materials

The components of the blends were commercial grades of polyamide 6 (PA 6, Ultramid B4, BASF AG) and a styrene-acrylonitrile copolymer (SAN, BASF AG), see Table 1. Before blending a styrene-acrylonitrile-maleic anhydride terpolymer (SANMA) which is miscible with SAN was added to the SAN grade. The SANMA content of the SAN grade was adjusted such that an absolute SANMA concentration of 3.4 wt.% was obtained for the three blends of this study. The terpolymer was composed of 2 wt.% maleic anhydride, 29 wt.% acrylonitrile and 69 wt.% styrene, and the weight average molecular weight of SANMA was 115 000 g/mol. On average, approx. 20 maleic anhydride groups were randomly located on the backbone of one SANMA chain.

Blend Preparation

We prepared three blends using a co-rotating twin screw extruder (Brabender, Duisburg, Germany). The diameter of the screws was 25 mm, the *L*/*D* ratio was 22, and the number of screw rotations was set to 50 min^{-1}. The weight fractions of PA 6 were 30% (abbreviated by PA 30), 50% (PA 50), and 70% (PA 70). The absolute weight fractions φ_i of PA 6, SAN and SANMA and the concentration of amino end groups c_{NH_2} and maleic anhydride groups c_{MA} are listed in Table 2 During melt mixing the maleic anhydride groups react with the amino end groups of PA 6, so that comb-like SANMA-*graft*-PA 6 chains are generated at the interface between PA 6 and SAN (see Figure 1). Recent investigations have shown that the reaction occurs in the initial stage of mixing shortly after melting of the solid pellets.[13,14]

Rheology

Linear viscoelastic oscillatory shear experiments were performed with cylindrical samples of a diameter of 22 mm using the shear rheometer UDS 200 (Physica, Stuttgart, Germany) in a parallel plates geometry (gap 1.8 mm). The measurements were conducted at $T = 240\,^{\circ}C$ in a nitrogen atmosphere. The shear amplitude was $\gamma_0 = 0.03$. Melt elongation experiments which were followed by a recovery interval were performed with rectangular samples of dimensions $56 \times 7 \times 2$ mm^3 using the Meissner-type uniaxial elongational rheometer RME at $T = 240\,^{\circ}C$.[15] The Hencky strain rates were $\dot{\varepsilon}_0 = 0.1\ s^{-1}$ and $\dot{\varepsilon}_0 = 0.3\ s^{-1}$. The maximum Hencky strain was $\varepsilon_{max} = 1.8$ which is equivalent to the stretch ratio $\lambda_{max} = \exp(\varepsilon_{max}) = 6.0$. In order to measure the recovered stretch, a pneumatically driven pair of scissors is installed in the RME. If the maximum strain $\varepsilon_{max} = 1.8$ at $\dot{\varepsilon}_0 = 0.3\ s^{-1}$ is attained, the scissors cut the sample at one boundary and the transient recovery of the sample could be measured by analysis of video sequences.

Morphology

Tapping mode atomic force microscopy (AFM) was applied to examine the morphology. Cut-offs of the samples were prepared and microtomed under cryo

Table 1.
Properties of the blend components.

	T_g (°C)	T_m (°C)	M_n (g/mol)	M_w (g/mol)	M_w/M_n	η_0 at 240 °C (Pa s)
PA 6	53	221	23000	121000	5.3	8400
SAN	109	–	57800	150000	2.6	2400

Table 2.
Composition of the PA 6/SAN blends.

Blend	Abbrev.	$\varphi_{PA\ 6}$ (wt.%)	φ_{SAN} (wt.%)	φ_{SANMA} (wt.%)	c_{NH_2} (mmol/kg)	c_{MA} (mmol/kg)
PA 6/SAN 70/30	PA70	70	26.6	3.4	30.4	7.3
PA 6/SAN 50/50	PA50	50	46.6	3.4	21.7	7.3
PA 6/SAN 30/70	PA30	30	66.6	3.4	13.0	7.3

conditions at $T = -120\ ^\circ C$. The microtomed surfaces were analyzed using the Nanoscope IIIa scanning probe microscope (Digital Instruments, Santa Barbara, USA).

Results

Linear Viscoelastic Shear Oscillations

The storage modulus G', the loss modulus G'', and the loss tangent $\tan\delta = G''/G'$ of the pure components and the PA 6/SAN blends as a function of frequency ω are presented in Figure 2. For the pure components the terminal behaviour of the Maxwell model with $G' \propto \omega^2$ and $G'' \propto \omega$ is almost reached at low frequencies. The dynamic moduli of the blends significantly differ from the pure components. At large frequencies, G' and G'' of the blends increase monotonically with PA 6 content. At low ω, the dynamic moduli of the blends are much larger than the values of the blend components. The linear viscoelastic behaviour of the PA30 and the PA50 blend is characterized by a convex shape of the log G' vs. log ω curve and a local maximum in tan δ (ω), and hence differs from the behaviour of the PA70 blend. Similar curves are frequently observed in suspension rheology and indicate that a ω independent plateau may exist at very low frequencies.[16–18] This tendency to form a low-frequency plateau in G' is not observed for the PA70 blend.

Melt Elongation and Recovery

Figure 3 presents the transient elongational viscosity μ (t) which is defined by

$$\mu(t) = \sigma(t)/\dot{\varepsilon}_0, \qquad (1)$$

where σ (t) denotes the measured tensile stress. The temperature was $T = 240\ ^\circ C$ and the Hencky strain rate was $\dot{\varepsilon}_0 = 0.1\ s^{-1}$ and $\dot{\varepsilon}_0 = 0.3\ s^{-1}$. The elongational viscosity of the pure components increases monotonically with time and attains a stationary value at large times (Figure 3a) which agrees well with the threefold of the zero

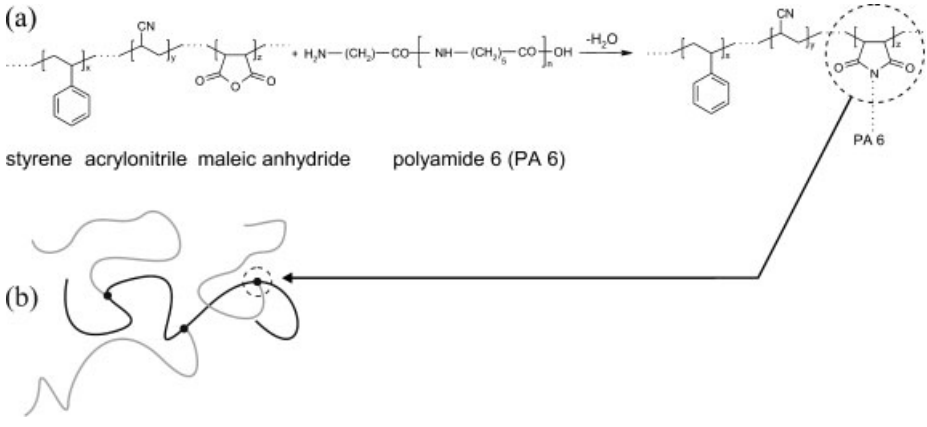

Figure 1.
(a) Compatibilizing reaction between SANMA and PA 6. (b) Scheme of a comb-like SANMA-*graft*-PA 6 molecule.

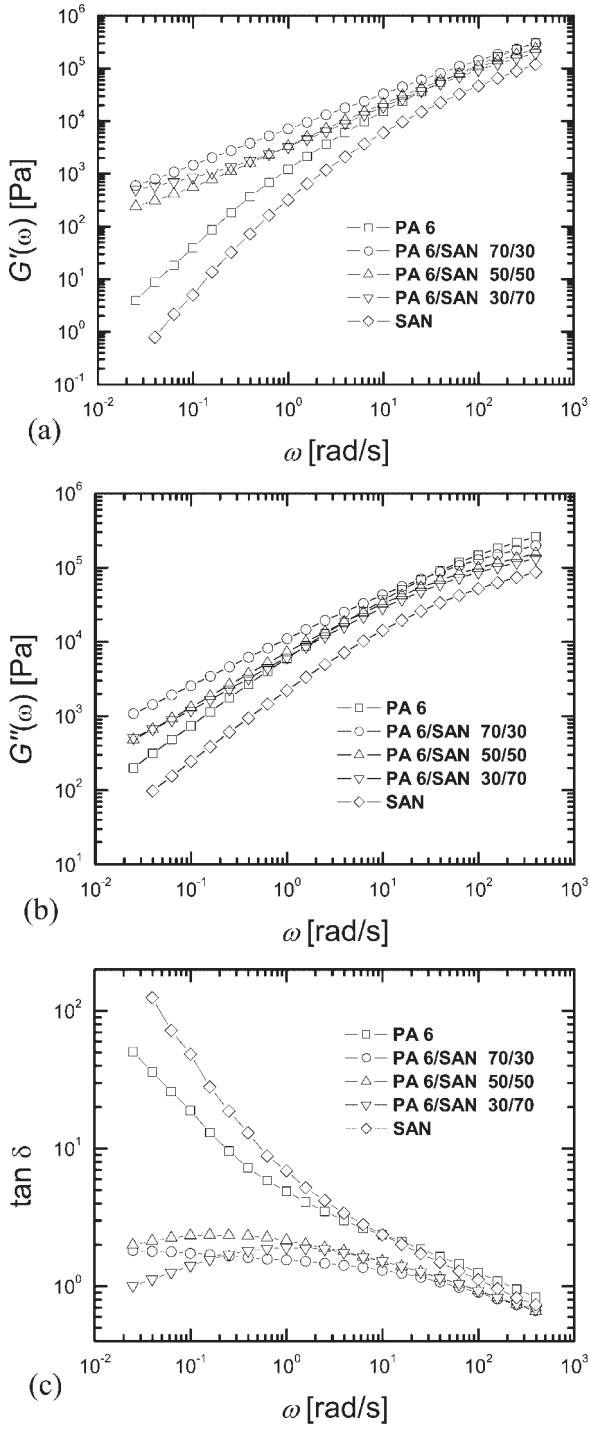

Figure 2.
(a) Storage modulus G', (b) loss modulus G'', and (c) damping factor tan δ as a function of frequency ω for PA 6 and SAN and the three different PA 6/SAN blends at $T = 240\ ^{\circ}C$. The weight fractions of PA 6 and SAN are indicated.

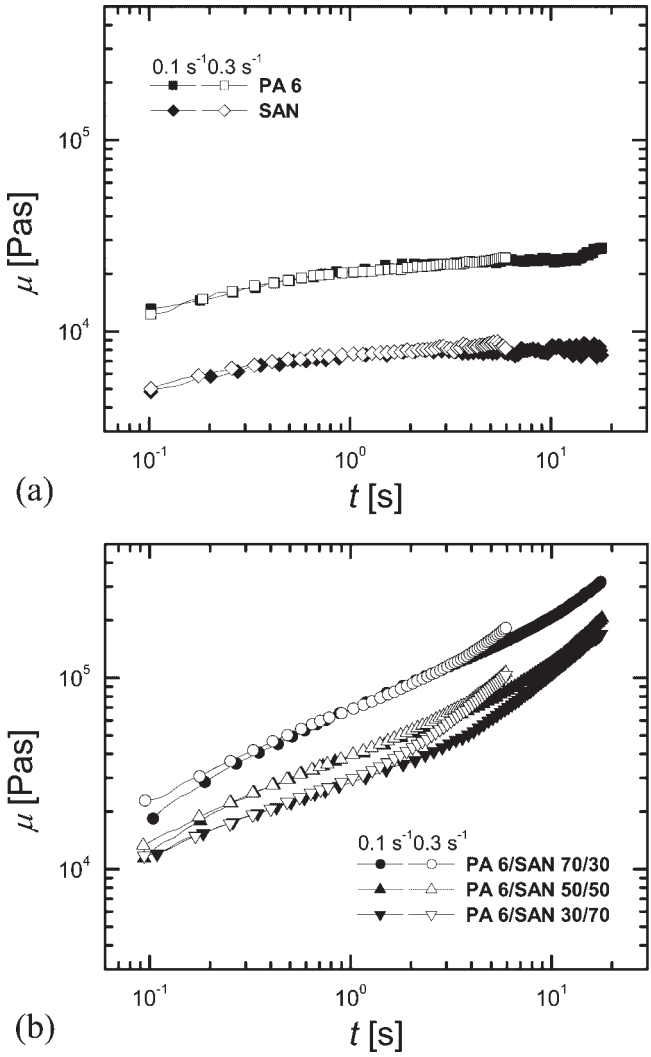

Figure 3.
Elongational viscosity μ as a function of time t at $T = 240\ ^{\circ}C$ for (a) PA 6 and SAN and (b) the three PA 6/SAN blends. The Hencky strain rate was 0.1 s^{-1} and 0.3 s^{-1}.

shear rate viscosity η_0. The elongational viscosity of the PA 6/SAN blends increases more rapidly than μ (t) of pure PA 6 and SAN and exceeds the viscosity of the single components at large times (Figure 3b). In contrast to the pure components and the PA70 blend, the μ (t) values for $\dot{\varepsilon}_0 = 0.1\ s^{-1}$ and $\dot{\varepsilon}_0 = 0.3\ s^{-1}$ of the PA50 blend and the PA30 blend strongly differ at larger times. This strain rate dependent behaviour is mostly pronounced for the PA30 blend where SAN forms the matrix phase.

At maximum Hencky strain $\varepsilon_{max} = 1.8$, the scissors cut the stretched sample and the transient recovered stretch λ_r

$$\lambda_r(t') = L_{max}/L(t') \quad (2)$$

of the blends was measured for $\dot{\varepsilon}_0 = 0.3\ s^{-1}$. In Equation 2 L_{max} denotes the length of the sample at cutting time $t = t_{max}$, and L (t') the length of the sample at recovery time $t' = t_{max}$. The recovered stretch λ_r of the pure components and the PA 6/SAN blends as a function of recovery time t' is presented

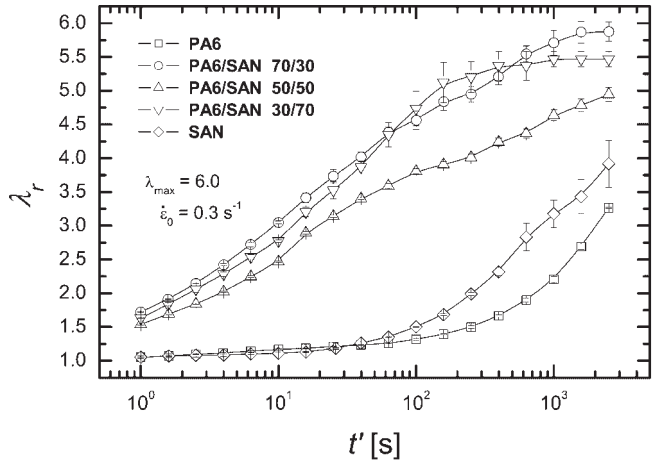

Figure 4.
Recovered stretch λ_r as a function of recovery time t' for PA 6 and SAN and the three different PA 6/SAN blends at $T = 204\,^{\circ}C$. The maximum Hencky strain was $\varepsilon_{max} = 1.8$, and the Hencky strain rate was $\dot{\varepsilon}_0 = 0.3\ s^{-1}$.

in Figure 4. The recovered stretch of the pure components is close to unity for $t' < 50$ s which shows that the polymer chains were not much stretched during melt elongation. For $t' > 50$ s the recovered stretch of the pure components increases and does not reach a stationary value within the measurement time. This effect can be explained by the surface tension of the sample and is more pronounced for SAN than for PA 6 because of the lower viscosity. The transient recovery of the blends differs considerably from the recovered stretch of PA 6 and SAN. The recovered stretch of all blends strongly increases for $t' < 50$ s and significantly exceeds the values of the blend components. The transient behaviour of the PA70 and the PA30 blend is similar. Both blends attain an almost stationary λ_r value for $t' > 1000$ s which corresponds to an almost completely reversible deformation $\lambda_r = \lambda_{max} = 6.0$. On the contrary, $\lambda_r\,(t')$ of the PA50 blend does not attain a stationary value and the value $\lambda_r\,(t') = 4.6$ at $t' = 42$ min is smaller compared to PA30 and PA70.

Morphological Investigations

In Figure 5, the dark phase is SAN and the bright phase is PA 6. The PA70 blend displays a disperse morphology with a bimodal distribution of spherical drops, see Figure 5(a). The disperse phase consists of droplets with radius of the order of 1 μm and a very large number of droplets with radii of less than 50 nm which are micelles and droplets with a high content of grafted SANMA chains. Recently, it was shown for a similar blend with 2 wt.% SANMA that coalescence between the droplets is strongly suppressed.[12] The morphology of the PA30 blend (Figure 5(c)) is very different from the PA70 blend. The PA 6 domains display a cluster-like shape which results from agglomeration during sample preparation.[12] In this case, compatibilization does not prevent agglomeration at large times, but tremendously delays coalescence. The PA50 blend exhibits a cocontinuous-like morphology (Figure 5(b)). Similar to the PA30 blend, the cluster-like character of the PA6 domains results from agglomeration and partial coalescence during sample preparation.[12]

Discussion

Reactive compatibilization strongly influences the linear viscoelastic properties of the blends. The low-frequency dynamic moduli of all blends were much larger than G' and G'' of the pure components. In case

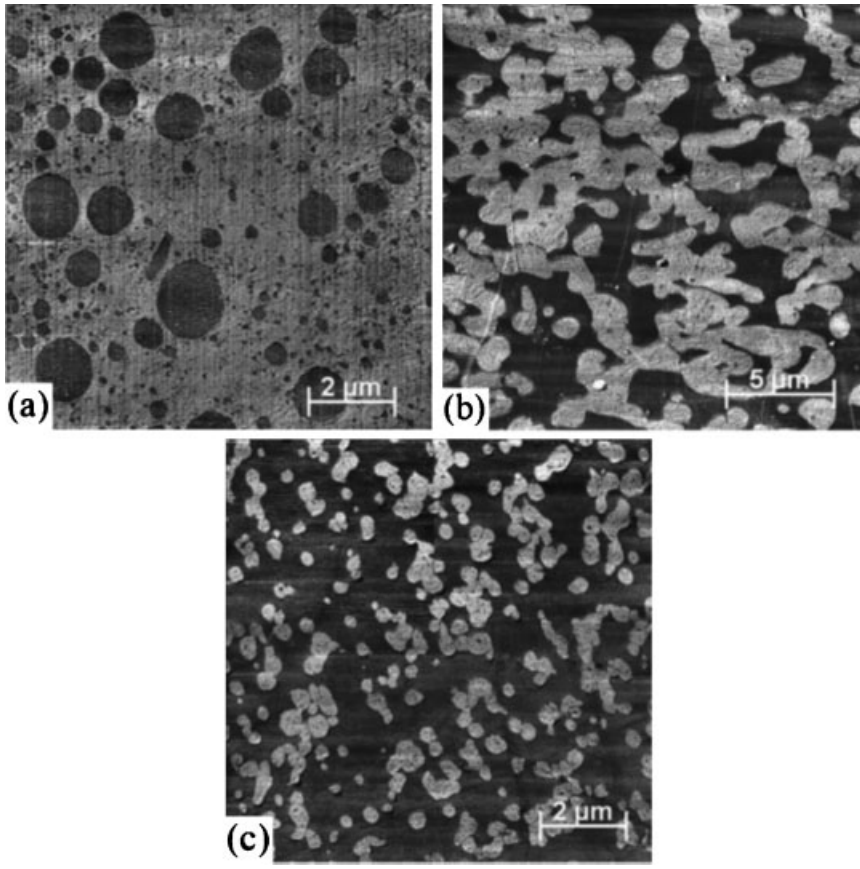

Figure 5.
Atomic force micrographs of (a) the PA 6/SAN 70/30 blend, (b) the PA 6/SAN 50/50 blend, and (c) the PA 6/SAN 30/70 blend after sample preparation.

of PA30 with the emulsion-type morphology this increase cannot be explained by the emulsion model of Palierne[19] if reasonable values of the interfacial tension α and the interfacial shear modulus β_{20} are used. For the blends of this study the compatibilizing reaction did not only change the interfacial properties between PA 6 and SAN, but also strongly changed the rheology of the bulk. Therefore the emulsion model is inapplicable. Furthermore, taking into consideration that surface grafting of particles can favor particle-particle interactions,[20,21] the appearance of the low-frequency plateau of PA30 and PA50 can be interpreted by elastic interactions between the grafted shells of the compatibilized PA 6 domains.

In comparison to uncompatibilized blends,[9] the transient elongational viscosity μ (t) of the reactively compatibilized blends does not obey a mixing rule for the viscosity of the blend components. Reactive compatibilization significantly increases the transient elongational viscosity of the blends and causes a non-linear, strain-hardening like behaviour. In recovery after melt elongation, the compatibilizing reaction between SANMA and PA 6 leads to an increase of the recovered stretch. Interestingly, the recovered stretch of the blends does not increase monotonically with PA 6 concentration. The blends with a disperse morphology display larger values of the recovered stretch than the cocontinuous

blend. This trend was also observed for uncompatibilized PS/PMMA blends.[9]

The differences in the morphological and rheological behaviour of the PA30 and PA70 blend give strong evidence of asymmetric interfacial properties which stem from the asymmetric molecular architecture of the in-situ generated multi-grafted SANMA chains. On the basis of the experimental observations we describe the interfacial situation as follows and point out that similar pictures of a reactively compatibilized interface were developed for comparable blend systems based on measurements of the interfacial thickness and TEM investigations.[22,23] The grafted PA 6 chains are identical to the bulk PA 6 and form a layer on the surface of the SAN droplets which stabilizes the drops against agglomeration and coalescence for the PA70 blend. Moreover, reactive compatibilization leads to the formation of an interphase with a considerable concentration of PA 6 on the surface of the PA 6 domains of the PA30 and the PA50 blend. The chemical composition of the interphase is different from the bulk SAN and favors aggregation of the PA 6 drops. The elastic interactions between these interphases of neighboring PA 6 particles cause the solid-like low frequency behaviour.

Conclusions

The interfacial reaction between maleic anhydride functionalized SAN and PA 6 strongly influences the viscous, elastic, and morphological properties of PA 6/SAN blends in the melt. In particular, the rheological and morphological properties of the PA30 blend differed significantly from the properties of the PA70 blend. We explained this observation by the asymmetric interfacial properties of the reactively compatibilized interface which origins from the asymmetric molecular architecture of the multi-grafted SANMA chains. On the one hand, the compatibilization reaction generates a layer of grafted PA 6 chains on the surface of SAN droplets which sterically stabilizes against droplet agglomeration and coalescence. On the other hand, it induces the formation of an interphase on the surface of the PA 6 domains. The differences in the chemical composition of the interphase compared to the bulk SAN favor aggregation of the PA 6 domains. The interactions between the interphases of neighboring PA 6 domains cause a solid-like low behaviour of the PA30 and the PA50 blend at low frequencies of the linear viscoelastic shear oscillations.

Acknowledgements: We thank Dr. M. Weber and Dr. H. Steininger (BASF AG, Ludwigshafen am Rhein, Germany) for stimulating discussions and for donation of the materials. The valuable discussions with Prof. J. Meissner and Prof. H. C. Öttinger and the support of W. Schmidheiny, F. Mettler, and J. Hostettler are gratefully acknowledged. The authors are also grateful to the Swiss National Science Foundation for financial support (Project-No. 200021-103287).

[1] L. A. Utracki, "*Polymer Alloys and Blends*", 2nd edition, Hanser, Munich **1989**.
[2] V. J. Triacca, S. Ziaee, J. W. Barlow, H. Keskkula, D. R. Paul, *Polymer* **1991**, *32*, 1401–1413.
[3] B. Majumdar, H. Keskkula, D. R. Paul, *Polymer* **1994**, *35*, 3164–3172.
[4] H. K. Jeon, J. K. Kim, *Macromolecules* **1998**, *31*, 9273–9280.
[5] S. H. Jafari, P. Pötschke, M. Stephan, H. Warth, H. Alberts, *Polymer* **2002**, *43*, 6985–6992.
[6] D. Graebling, R. Muller, J. F. Palierne, *Macromolecules* **1993**, *26*, 320–329.
[7] H. Gramespacher, J. Meissner, *Journal of Rheology* **1992**, *36*, 1127–1141.
[8] I. Vinckier, P. Moldenaers, J. Mewis, *Journal of Rheology* **1996**, *40*, 613–631.
[9] U. A. Handge, P. Pötschke, *Journal of Rheology* **2004**, *48*, 1103–1122. *Erratum* **2005**, *49*, 1553.
[10] H. Asthana, K. Jayaraman, *Macromolecules* **1999**, *32*, 3412–3419.
[11] M. Moan, J. Huitric, P. Mederic, J. Jarrin, *Journal of Rheology* **2000**, *44*, 1227–1245.
[12] C. Sailer, U. A. Handge, *Macromolecules* **2007**, *40*, 2019–2028.
[13] M. van Duin, A. V. Machado, J. Covas, *Macromolecular Symposia* **2001**, *170*, 29–39.
[14] M. Weber, W. Heckmann, A. Goeldel, *Macromolecular Symposia* **2006**, *233*, 1–10.
[15] J. Meissner, J. Hostettler, *Rheologica Acta* **1994**, *33*, 1–21.

[16] T. Masuda, A. Nakajima, M. Kitamura, Y. Aoki, N. Yamauchi, A. Yoshioka, *Pure and Applied Chemistry* **1984**, *56*, 1457–1475.
[17] P. Bardollet, M. Bousmina, R. Muller, *Polymers for Advanced Technologies* **1995**, *6*, 301–308.
[18] U. A. Handge, P. Pötschke, *Rheologica Acta* **2007**, online (10.1007/s00397-007-0179-6).
[19] J. F. Palierne, *Rheologica Acta* **1990**, *29*, 204–214.
[20] Y. Aoki, *Macromolecules* **1987**, *20*, 2208–2213.
[21] M. Fahrländer, M. Bruch, T. Menke, C. Friedrich, *Rheologica Acta* **2001**, *40*, 1–9.
[22] S. Yukioka, T. Inoue, *Polymer* **1994**, *35*, 1182–1186.
[23] A. Steurer, G. P. Hellmann, *Polymers for Advanced Technologies* **1998**, *9*, 297–306.

